Extraction of Transmission Line Surface Roughness Using S-Parameter Measurements and Cross-Sectional Information

Ze Sun[®], *Student Member, IEEE*, Jian Liu, Xiaoyan Xiong, DongHyun Kim[®], *Member, IEEE*, Daryl Beetner[®], *Fellow, IEEE*, and Victor Khilkevich[®], *Member, IEEE*

Abstract—The intentional roughness created on conductor surfaces during the printed circuit board (PCB) manufacturing process leads to a substantial increase of conductor loss at frequencies in the order of tens of gigahertz. It is essential to know the roughness of PCB conductors to create adequate models of the high-speed channels. This article presents a novel method for extracting the roughness level of conductor foils using only measured S-parameters and cross-sectional information. The proposed technique is relatively easy to perform, cost-effective, and does not require the destruction of test boards, making it a promising alternative to existing methods that rely on optical or scanning electron microscope imaging. Besides, the proposed method can handle boards with nonequal roughness on different conductor surfaces, which is common in PCBs. The method is validated through both simulation and measurement, and a good correlation is achieved between the extracted roughness level and the values obtained by microscopic imaging.

Index Terms—Printed circuit board (PCB), signal integrity, striplines, surface roughness.

I. INTRODUCTION

N THE assessment of the signal integrity performance of high-speed channels, a precise characterization of conductor loss is critical. The application of skin effect formulas for calculating conductor loss assumes smooth conductor surfaces. Nevertheless, in the process of printed circuit board (PCB) manufacturing, roughness is intentionally induced on conductor surfaces to enhance adhesion to the dielectric material. At frequencies in the order of tens of gigahertz, the disregard of surface roughness can result in a substantial underestimation of conductor loss [1]. Hence, it is crucial to consider the impact of surface roughness when evaluating the conductor loss of high-speed channels.

Several techniques have been proposed to compute the additional conductor loss resulting from rough surfaces [2], [3].

Manuscript received 28 June 2023; revised 2 November 2023 and 27 December 2023; accepted 30 January 2024. Date of publication 5 February 2024; date of current version 22 February 2024. This work was supported in part by the National Science Foundation under Grant IIP-1916535. (Corresponding author: Ze Sun.)

Ze Sun, DongHyun Kim, Daryl Beetner, and Victor Khilkevich are with the Missouri University of Science and Technology, Rolla, MO 65409 USA (e-mail: sunz1@umsystem.edu; dkim@mst.edu; daryl@mst.edu; khilkevichv@mst.edu).

Jian Liu and Xiaoyan Xiong are with the Cadence Design Systems Inc., San Jose, CA 95134-1931 USA (e-mail: jliu@cadence.com; xiongx@cadence.com). Digital Object Identifier 10.1109/TSIPI.2024.3361863

Although the mathematical aspects employed in each technique vary, they all follow a similar process. Initially, a microsectioned sample of the PCB is produced and imaged via either an optical or scanning electron microscope (SEM), depending on the desired resolution [4]. Subsequently, the rough foil is modeled utilizing simple geometric structures, such as wedges [5], spheres, or semispheres [6], with the size of the structure being determined by the profile of the conductor surface obtained in the first step. Finally, the additional conductor loss introduced by the protruding structures is calculated analytically. The ratio between the per-unit-length (PUL) resistance of the transmission line with rough and smooth conductor surfaces is referred to as the surface roughness correction factor K [7]

$$K = \frac{R_{\text{rough}}}{R_{\text{smooth}}}.$$
 (1)

The primary challenge associated with calculating the correction factor K from the conductor surface profile information is the requirement for manufacturing and photographing a PCB sample in advance. This process is cost- and time-consuming and requires the use of specialized optical or SEM equipment, which may not be readily accessible in many RF laboratories.

Previous studies have proposed methods for extracting surface roughness without resorting to SEM or optical microscopic measurement, such as [8]. However, this approach models the frequency dependency of both dielectric and conductor loss using the "root-omega" method [9], which may inaccurately characterize the dielectric loss tangent as reported in the article. In [10], the dielectric loss was calculated using the permittivity and loss tangent values provided by the vendor at a single frequency, which does not hold true in practice. Furthermore, these studies assumed uniform roughness levels across all conductor surfaces, an assumption which may not accurately reflect the real-world PCB manufacturing conditions. Specifically, the sides attached to the core laminate are typically rougher, as demonstrated in Fig. 1, to ensure improved adhesion. In such scenarios, assuming the same level of roughness across all surfaces is no longer accurate. Instead, distinct correction factors must be assigned to each surface. In our previous work [11], we introduced a methodology for optimizing the roughness level of different conductor surfaces. This was achieved by interactively adjusting the roughness levels in the cross-sectional analysis model and minimizing the difference between the simulated

2768-1866 © 2024 IEEE. Personal use is permitted, but republication/redistribution requires IEEE permission. See https://www.ieee.org/publications/rights/index.html for more information.



Fig. 1. Optical microscopic image of a stripline trace cross section. The roughness levels on the top and bottom surfaces are noticeably different.

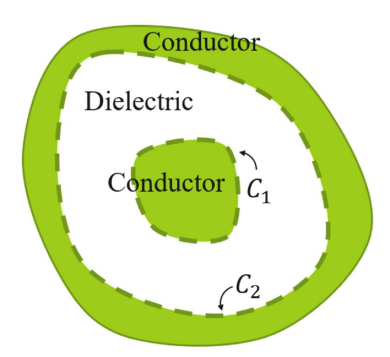


Fig. 2. Cross section of an arbitrary two conductor transmission line.

PUL resistance and the target. The validation of this method demonstrated accurate extraction results. However, this method has a drawback of being time-consuming, requiring several hundreds of iterations to obtain optimized results.

In this article, a novel surface roughness characterization method is introduced. The proposed technique entails the determination of roughness level on distinct conductor surfaces, based on the S-parameter measurements and the cross-sectional geometry of the test board. In comparison to the optical or SEM imaging, S-parameter measurement is a simpler process that does not require the destruction of test boards to produce cross sections. Therefore, this approach saves both time and money during the extraction process.

This rest of this article is organized as follows. First, in Sections II and IV, the analytical equations used to extract roughness level from the measurement S-parameter and cross-sectional analysis are derived. Next, in Sections III to VI, the details of the extraction process are presented. Then, in Section VII, the proposed method is validated using a fabricated PCB board. Finally, Section VIII concludes this article.

II. EXTRACTION METHODOLOGY

In transmission lines, the PUL power loss that results from the conductivity of metallic conductors can be determined by the following equation [12]:

$$P_c = \frac{R_s}{2} \int_{C_1 + C_2} \bar{H} \cdot \bar{H}^* dl \tag{2}$$

where R_s is the surface resistance of the conductor (assuming equal resistances on all surfaces), \bar{H} is the magnetic field, and C_1 and C_2 are the integration paths around the conductor boundaries, as shown in Fig. 2.

On the other hand, the PUL power loss can also be represented through circuit theory, where I_0 is the total current flowing through the transmission line

$$P_c = R \frac{|I_0|^2}{2}. (3)$$

By substituting (3) to (2), the PUL resistance R can be expressed in terms of the magnetic field \bar{H} of the transmission line and the surface resistance of the conductors

$$R = \frac{R_s}{|I_0|^2} \int_{C_1 + C_2} \bar{H} \cdot \bar{H}^* dl = R_s A \tag{4}$$

where A is a coefficient defined as

$$A = \frac{1}{I_0^2} \int_{C_1 + C_2} \bar{H} \cdot \bar{H}^* dl.$$
 (5)

When the surface of the transmission line is smooth, the surface resistance R_s can be approximated by the skin-effect formula

$$R_s = \frac{1}{\sigma \delta} = \sqrt{\frac{\omega \mu}{2\sigma}} \tag{6}$$

where σ is the conductivity of the conductor, δ is the skin depth, ω is the angular frequency, and μ is the permeability of the conductor.

For a transmission line with rough surfaces, a surface roughness correction factor K (1) is introduced to account for the additional conductive loss caused by the rough surface. This factor is related to the level of surface roughness. In this study, the relationship between K and the surface roughness geometry is described using the Huray model, which, according to the previous study, demonstrates good accuracy for frequencies up to 50 GHz [7], [13]

$$K = 1 + 1.5 \cdot \text{SR} \cdot \frac{1}{1 + \frac{\delta}{a} + \frac{1}{2} \left(\frac{\delta}{a}\right)^2} \tag{7}$$

where a is the effective radius of the spherical protrusions, and SR is the Hall-Huray surface ratio, which is defined as

$$SR = \frac{4\pi Na^2}{A_{\text{smooth}}} \tag{8}$$

where N represents the number of spheres contained within the tile of area $A_{\rm smooth}$. The value of SR quantifies the distribution density of spheres. In this study, it is assumed that two adjacent spheres are positioned side-by-side on the smooth plane, as depicted in Fig. 3. As a result, the value of $A_{\rm smooth}$ for one periodic unit is equal to $(2a)^2$, and N=1. Therefore, according to (8), the value of SR is π .

As defined by (1), K represents the ratio of the PUL resistance R of transmission lines with a rough surface to that of transmission lines with a smooth surface. Furthermore, as will be shown in Section VI, the coefficient A in (4) exhibits a weak dependence on the surface roughness. Consequently, by substituting (4) into (1), the surface resistance R_s of the rough surface can be expressed as

$$R_s \approx K \sqrt{\frac{\omega \mu}{2\sigma}}. (9)$$

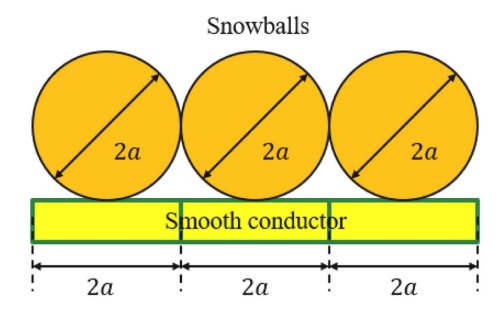


Fig. 3. Spheres are placed on top of a smooth conductor and right next to each other according to Huray model.

As mentioned in the introduction, it is commonly observed that various surfaces of a PCB board may possess different levels of roughness due to technological needs. For n different roughness levels on different surface segments of the transmission line cross section (e.g., top, sides, and bottom surfaces of the trace, and the surfaces of the return planes), by extension of (4), the PUL R can be expressed as the cumulative contribution of all segments, resulting in the following formula:

$$R = \sum_{i=1}^{n} R_{si} \frac{1}{I_0^2} \int_{C_i} \bar{H} \cdot \bar{H}^* dl = \sum_{i=1}^{n} R_{si} A_i$$
 (10)

where C_i is the integration path over the boundary of the *i*th segment, R_{si} is the corresponding surface resistance of that segment, and the coefficient A_i is defined as

$$A_i = \frac{1}{I_0^2} \int_{C_i} \bar{H} \cdot \bar{H}^* dl.$$
 (11)

The n unknown surface resistances R_{si} are the quantities that need to be found to determine the surface roughness of the transmission line conductors. It is possible to write m equations (10) for m different transmission lines that differ in geometry but have the same set of conductor segments with the same surface resistances. In the process, the following system of equations will be composed:

$$\begin{cases}
R_{s1}A_{11} + \dots + R_{si}A_{1i} + \dots + R_{sn}A_{1n} = R_1 \\
\vdots \\
R_{s1}A_{j1} + \dots + R_{si}A_{ji} + \dots + R_{sn}A_{jn} = R_j \\
\vdots \\
R_{s1}A_{m1} + \dots + R_{si}A_{mi} + \dots + R_{sn}A_{mn} = R_m
\end{cases}$$
(12)

where the coefficients A_{ji} pertain to the segment i of the transmission line j, and R_j is the PUL resistance of the transmission line j. If the coefficients A_{ij} are independent of the surface resistances R_{si} (which is only approximately true as will be shown later), the system (12) is linear with respect to R_{si} with a unique solution existing for $m \geq n$ (if the equations in the system are linearly independent). The equation system (12) can also be represented in the matrix form as follows:

$$[A][R_s] = [R]. \tag{13}$$

The elements of the matrix [A] can be filled by calculating the H field for each geometry and then using (11). The [R] vector can be extracted from the S-parameter measurement, which is discussed in Section III.

A possible misunderstanding of (12) is that, since the PUL resistance of the transmission line is the sum of the integrals along the segments of the conductor surfaces (e.g., top, bottom, left, and right sides), increasing the perimeter of the signal trace cross section will lead to a larger PUL resistance, which is nonphysical. The coefficients A_{ij} in (12) are determined by the H field distribution on the conductor surface. This distribution is, in turn, determined by the cross-sectional geometry of the transmission line. The increase of the conductor perimeter increases the integration path, but at the same time, the magnetic field at the surface of the conductor decreases, resulting in smaller values of A_{ij} . Equation (12), therefore, does not imply an increase in resistance with a larger conductor perimeter but rather outlines the relationship between the cross-sectional geometry and the resulting PUL resistance.

It is important to note, however, that in real-world applications the geometries of the transmission lines used to build the system of equations in (12) may result in ill-conditioned equations. This means that errors introduced in the measurement and simulation process can cause unacceptable inaccuracies in the solution. This issue is discussed in Section IV. A further issue is that the [A] matrix cannot be assumed to be entirely independent of surface roughness, which is addressed in Section VI.

III. EXTRACTION OF PUL R From S-Parameters

To extract the PUL resistance R from the S-parameters in real measurements, the first step is to de-embed the measured S-parameters (i.e., the effects of test fixtures are removed and the S-parameters are normalized to the actual impedance of the line). In this study, a variant of the 2x thru de-embedding technique known as "eigenvalue de-embedding" [14] is employed. This de-embedding technique was chosen due to its precision in handling translationally uniform transmission lines and its utilization of a minimal number of standards, requiring only two lines of different lengths. After de-embedding, the obtained transmission coefficient will depend only on the propagation constant γ and the length of the line l

$$S_{21} = e^{\gamma l} = e^{(\alpha + j\beta)l}. (14)$$

The total attenuation factor α of the transmission line can be extracted from the amplitude of the de-embedded transmission coefficient as

$$\alpha = \frac{-\ln[|S_{21}|]}{l}.\tag{15}$$

Subsequently, the loss tangent $\tan \delta$ and the relative permittivity ε_r of the dielectric layer can be extracted through the method described in [15] and [16]. This extraction process requires two transmission lines with different geometries, which can also can be used later to extract different roughnesses on the matte and drum sides of the foils (see Section IV). With the obtained dielectric material information, the dielectric loss ($\alpha_{\rm diel}$) can be

calculated using the following equation:

$$\alpha_{\text{diel}} = \frac{1}{2} \cdot \tan \delta \cdot \omega \cdot \sqrt{LC} \tag{16}$$

where C and L represent the PUL capacitance and inductance of the transmission line, which are obtained through the 2-D analysis of transmission line assuming smooth conductor surfaces.

The conductor loss α_{cond} of the transmission line can then be calculated as follows [12]:

$$\alpha_{\rm cond} = \alpha - \alpha_{\rm diel}.$$
 (17)

For low loss transmission lines, α_{cond} can further be expressed using the PUL parameters as follows [12]:

$$\alpha_{\rm cond} \approx \frac{1}{2} R \sqrt{\frac{C}{L}}.$$
 (18)

In this way, the PUL R of the transmission line can be finally obtained as follows:

$$R = 2\alpha_{\rm cond} \sqrt{\frac{L}{C}}.$$
 (19)

IV. SENSITIVITY TO ERRORS AND SELECTION OF THE TEST VEHICLE GEOMETRY

In principle, the surface roughness can be extracted by solving the linear system (13). It is important, however, to ensure that the sensitivity of the solution to the measurement errors is at an acceptable level.

The right-hand side of (13) is determined by the measurement and, thus, can contain significant amount of errors. Let us define the perturbed right-hand side vector of (13) as

$$[R'] = [R] + [\delta R] \tag{20}$$

where $[\delta R]$ is the perturbation vector. Solving the equation $[A][R_s'] = [R']$ with the perturbed left-hand side will produce the perturbed solution

$$[R'_s] = [R_s] + [\delta R_s].$$
 (21)

The sensitivity of the solution to the errors then can be defined as the ratio of the relative perturbations of the left-hand side and the solution vectors

$$S_e = \frac{||[\delta R_s]||}{||[R_s]||} / \frac{||[\delta R]||}{||[R]||}.$$
 (22)

In the case of the linear system of equations, the sensitivity to the errors is equal to the condition number of the matrix [A]

$$\kappa = \|[A]\| \|[A]^{-1}\|. \tag{23}$$

Each equation in (12) and (13) is constructed using a unique transmission line geometry. To establish a well-conditioned system of equations, the \bar{H} field distribution of these transmission lines must be as orthogonal as possible. This can be achieved by using designs with significantly different layer stackups and layouts. For stripline configurations, variations can be made to the following geometric parameters: the trace width, trace thickness, core thickness, and prepreg thickness. Among them, the trace thickness is difficult to change significantly in practice. To investigate the effect of the variations in the remaining

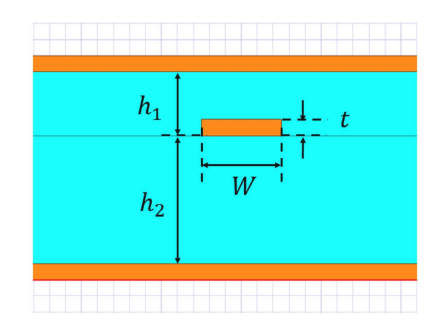


Fig. 4. Stripline model and its geometrical parameters.

TABLE I
CONFIGURATIONS OF SINGLE-ENDED STRIPLINES UNDER SIMULATION

Dimensions (mil)	t	W	h1	h2
TL 1	1	5	4	8
TL 2	1	5	8	4
TL 3	1	25	4	8

TABLE II CONDITION NUMBER OF THE MATRIX [A] CREATED USING DIFFERENT GEOMETRY COMBINATIONS

Geometry	Condition number	
Single-ended TL 1, TL 2	4.16	
Single-ended TL 1, TL 3	125.55	
Single-ended TL 2, TL 3	5.60	
Coupled stripline	58.65	

geometrical parameters on the condition number of (12), several transmission line geometries were created.

The first group of examples presents pairs of single-ended striplines with different cross-sectional geometries, as depicted in Fig. 4. The specifications of the transmission lines, including the thickness of the trace and ground (t), the width of the trace (W), and the thickness of the core (h1) and prepreg (h2), are summarized in Table I. Among them, transmission lines TL 1 and TL 2 have the same trace thickness and width but use different stackups, while transmission lines TL 1 and TL 3 have the same trace thickness and stackup but differ in the trace width. Two different levels of surface roughness were assigned to the conductors. Specifically, the drum side (which includes the top reference ground, top surface, and side walls of the trace) has a roughness level of $0.5~\mu m$, while the matte side (which includes the bottom reference ground and the bottom surface of the trace) possesses a roughness level of $3~\mu m$.

The transmission lines were simulated at 2 GHz using the Ansys Q2D solver. For each of the geometries, the coefficients A were calculated. Since there are three geometries and two unknown surface resistances, three different systems of equations can be created by different combinations of TL1, TL2, and TL3. The condition numbers of all three combinations are calculated using (23), and the results are given in Table II.

As can be seen, the condition numbers differ significantly depending on the geometry combination. Using two lines with

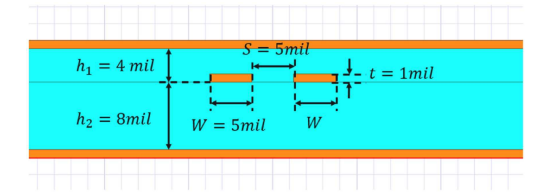


Fig. 5. Cross-section of the coupled stripline model.

different stackups, but with the same trace width resulted in a condition number that is 24–30 times smaller than the condition number of the combination of lines using the same stackup and a different trace width. These results mean that the sensitivity to measurement errors is significantly different for different geometry combinations. Combinations 1 and 3 demonstrate an acceptable error sensitivity (for example, a 3% error in the R vector will propagate to a 12%–17% error in the solution), while for the combination 2 the sensitivity is unacceptably high (the same 3% error will propagate to a 370% error in the solution).

As can be seen from the table, varying the board stackup can result in a relatively low error sensitivity, suitable for surface resistance extraction. In practical applications, however, when constructing two striplines with different stackups, the roughness of different copper layers cannot be maintained at the same level due to manufacturing limitations. This would violate the condition that the surface resistance of the conductive segments should remain the same for each transmission line geometry, and the system of equations would become inconsistent. In this case, only the trace width can be varied, but this results in unacceptably high error sensitivity.

Another possibility to generate a geometry for the solution of the system (12) is to use the common and differential modes in a coupled stripline pair. An example of such a configuration is shown in Fig. 5. The corresponding equation system exhibits a condition number of 58.65, which is better than for the combination of the single-ended striplines of different widths (Table II), but is still high.

The results presented in this section demonstrate that the applicability of system (12) for extraction of the surface resistances is limited by the error sensitivity, and while the geometries providing acceptable sensitivity levels exist, they are not always practically manufacturable. This sensitivity to errors can be significantly reduced, however, if the linear system (12) is replaced by a nonlinear system of equations.

V. EXTRACTING SURFACE ROUGHNESS BY SOLVING A NONLINEAR SYSTEM OF EQUATIONS

To formulate a nonlinear system of equations, the frequency-dependency of the loss associated with roughness can be taken into account. To do this, the equations in (12) are written at p discrete frequencies and are appended with the Huray formula (7), relating the values of the surface resistances at these frequencies to the size of the protrusion spheres on the corresponding surfaces. In this way, a system of nonlinear equations with respect to the unknown radii a_i of each surface segment is

established

$$\begin{cases}
R_{s1}(\omega_{1})A_{11}(\omega_{1}) + \dots + R_{sn}(\omega_{1})A_{1n}(\omega_{1}) = R_{1}(\omega_{1}) \\
\vdots \\
R_{s1}(\omega_{q})A_{j1}(\omega_{q}) + \dots + R_{sn}(\omega_{q})A_{jn}(\omega_{q}) = R_{j}(\omega_{q}) \\
\vdots \\
R_{s1}(\omega_{p})A_{m1}(\omega_{p}) + \dots + R_{sn}(\omega_{p})A_{mn}(\omega_{p}) = R_{m}(\omega_{p}) \\
\vdots \\
R_{si}(\omega_{q}) = \left[1 + \frac{1.5\pi}{1 + \frac{\delta_{q}}{a_{i}} + \frac{1}{2}\left(\frac{\delta_{q}}{a_{i}}\right)^{2}}\right] \sqrt{\frac{\omega_{q}\mu}{2\sigma}}
\end{cases}$$
(24)

The system can be solved by any suitable nonlinear optimization method. In this work the pattern search algorithm is employed to solve this system [17], optimizing an objective function defined as

$$\Delta = \frac{\| [R] - [R'] \|}{\| [R] \|}.$$
 (25)

This objective function quantifies the relative error between the target PUL [R] of the transmission line and the PUL vector [R'] calculated at each iteration of the optimization process.

To demonstrate the robustness of the reconstruction results against errors originating from *S*-parameter measurements and 2-D numerical calculations, the coupled stripline configuration illustrated in Fig. 5 was simulated at three distinct frequencies (2, 6, and 10 GHz).

To evaluate the sensitivity of the solution to errors, a statistical analysis was conducted. The fluctuations in $[\delta R]$ were assumed to follow a Gaussian distribution with zero mean value and a standard deviation equal to 1% of the values of the elements of [R], meaning that the values of $[R+\delta R]$ are within 3% of [R] with 99% probability. Five thousand tests were performed, resulting in a mean value of the sensitivity to errors equal to 4.11. This value is comparable to the condition number obtained from the equation system built with single-ended traces with different dielectric layer thicknesses (TL 1 and TL 2), providing a practical way to extract the surface roughness.

VI. ITERATIVE OPTIMIZATION

In the previous examples, [A] was determined using the simulation result of transmission lines with known roughness levels. Since the matrix [A] is dependent on the surface resistance of the conductors (at least when the Q2D solver is used), in real applications, the elements of [A] need to be calculated with a certain assumed roughness. Nonetheless, the dependency of the elements of the matrix [A] on the resistance is relatively weak and (24) can be seen as a linearization of the actual system of equations around the current values of [a]. As such it is possible to solve (24) iteratively, using the solution from the previous iteration to calculate the matrix [A] at the current iteration.

To illustrate the impact of the surface roughness on matrix [A], a series of simulations were conducted for the coupled stripline shown in Fig. 5. The roughness level of the drum side was fixed as 0.5 μ m, and the roughness of the matte side was varied from

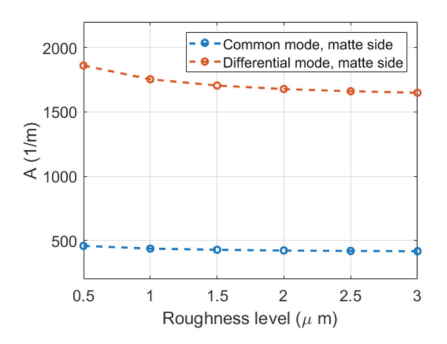


Fig. 6. Change of the elements of the matrix A with surface roughness.

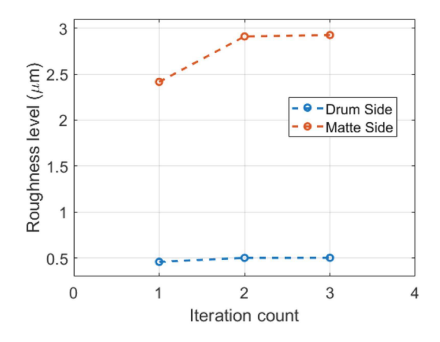


Fig. 7. Change in the extracted roughness by iteratively solving (24).

0.5 to $3 \mu m$, with a step size of $0.5 \mu m$. The resulting changes in the elements of the matrix [A] corresponding to the matte side at 2 GHz are shown in Fig. 6. As the surface resistance increases, the values of the elements of the matrix A gradually decrease.

The iterative algorithm was applied to the coupled stripline to demonstrate its accuracy. Initially the matrix [A] was calculated using the transmission line model with the smooth surface. At each iteration, the system of equation (24) was solved by the pattern search algorithm, and the obtained solution [a] was used to calculate the matrix [A] for the next iteration. The change in the extracted roughness level a over the iteration is presented in Fig. 7. The iterative algorithm was stopped when the relative difference of the solution between the consecutive iterations falls below a certain predefined threshold. In this example, the 1% convergence threshold was reached after three iterations, and the final extraction result of roughness levels were $0.50~\mu m$ for the drum side and $2.93~\mu m$ for the matte side, which agrees well with the true values $(0.50~and~3~\mu m)$.

VII. EXPERIMENTAL VALIDATION OF THE PROPOSED METHOD

To validate the proposed surface roughness extraction method, a test vehicle containing a pair of differential striplines was fabricated with lengths of 1 and 5 in. The cross-sectional geometry of the transmission line is shown in Fig. 8. First, the optical microscopic measurement was performed to extract roughness profiles of the conductors. Utilizing the roughness extraction tool presented in [18], the root-mean-square (rms) roughness level for the top ground, top surface, and side walls of the trace (drum side) were found to be $0.55~\mu m$, while the

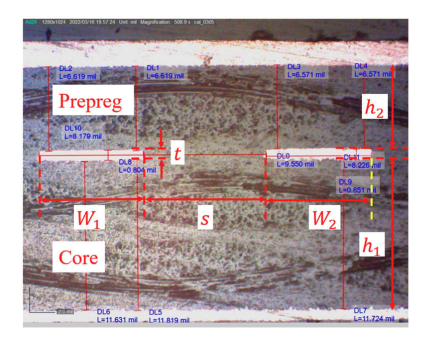


Fig. 8. Cross section of the coupled striplines used in experimental validation. The trace width $(W_1 = W_2)$ is $8.20 \ mil$; edge-to-edge spacing (s) is $9.55 \ mil$; prepreg height (h_1) is $6.59 \ mil$; core thickness is $11.72 \ mil$; trace thickness (t) is $0.82 \ mil$.

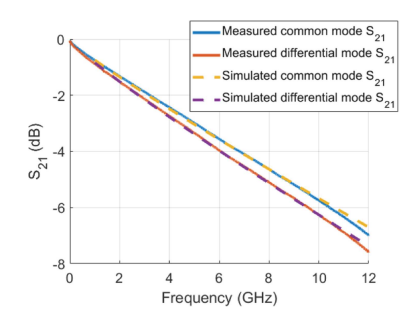


Fig. 9. De-embedded common and differential transmission coefficients.

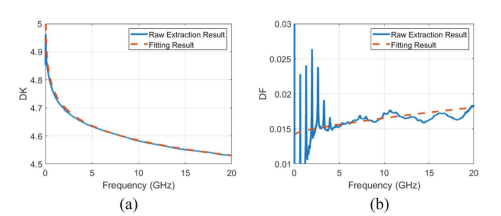


Fig. 10. Extracted (a) dielectric constant and (b) loss tangent of the test board.

bottom reference ground and the bottom surface of the trace (matte side) exhibited a roughness level of 1.26 μ m.

The S-parameters of the stripline were measured. The amplitudes of the de-embedded S_{21} for both the common mode and differential mode are presented in Fig. 9 (solid lines). The permittivity and loss tangent of the dielectric material were obtained from the transmission coefficients using the methodology reported in [15], (Fig. 10). As reported in [15], accurate extraction of these parameters at lower frequencies is challenging due to increased susceptibility to measurement and simulation errors. To mitigate the unrealistic fluctuations observed at low frequencies, the two-term Djordjevic model introduced in [15] was employed to fit the extracted permittivity and loss tangent. They are represented in Fig. 9 be dashed lines. The PUL R was extracted using the process described in Section III, and is shown in Fig. 11.

The roughness levels of the drum side and matte side of the board were then extracted following the iterative workflow presented in Section VI. To mitigate the error introduced in

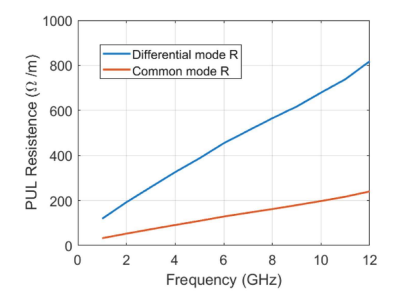


Fig. 11. Extracted PUL R of the common mode and differential mode of the stripline shown in Fig. 8.

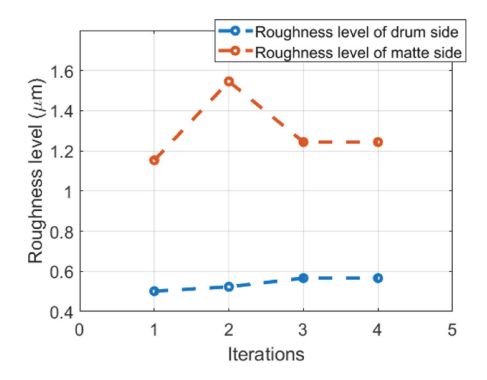


Fig. 12. Change in the roughness level determined for the test vehicle during the iterative solution.

the S-parameter measurement, the system (24) was written at three frequencies (2, 6, and 10 GHz). The convergence criteria was defined as a 1% difference in the extraction results between successive iterations. After four iterations, the extraction result converged, as shown in Fig. 12. During each simulation, the majority of the computational time was spent on the 2-D cross-sectional analysis, which required approximately ten sections. After that, the solution of the equation system was achieved within a single second. The reconstructed roughness levels for the drum and matte sides were found to be 0.56 and 1.24 μ m, respectively, which is within 1.7% of the values determined by cross-sectioning (0.55 and 1.26 μ m).

Using the extracted roughness and dielectric parameters, the modal transmission coefficient of the differential stripline was calculated using the 2-D cross-sectional simulator (Q2D). As shown in Fig. 9 (dashed line), the simulated transmission coefficients correlate well with the measurement. This suggests that the extracted roughness parameters provide an accurate model for the additional conductor loss introduced by surface roughness.

VIII. CONCLUSION

This article proposes a novel method for accurately characterizing the roughness level of conductor foils in PCBs. The size of protrusions on different conductor surfaces can be determined separately using *S*-parameter measurements and the cross-sectional geometry of the board, without the requirement

of microscopic surface roughness imaging. The sensitivity of the method was thoroughly analyzed through its application to various geometries. In the end, a well-conditioned system of nonlinear equations was established and experimentally validated on a differential stripline demonstrating high accuracy of the roughness parameter extraction. Compared to existing methods that rely on optical or SEM imaging, the proposed technique is much easier to perform, cost-effective, as it does not necessitate the destruction of test boards to produce cross sections.

REFERENCES

- P. G. Huray et al., "Fundamentals of a 3-D "snowball" model for surface roughness power losses," in *Proc. IEEE Workshop Signal Propag. Inter*connects, 2007, pp. 121–124.
- [2] P. G. Huray, O. Oluwafemi, J. Loyer, E. Bogatin, and X. Ye, "Impact of copper surface texture on loss: A model that works," in *DesignCon*, vol. 1, pp. 462–483, 2010.
- [3] X. Guo, D. R. Jackson, M. Y. Koledintseva, S. Hinaga, J. L. Drewniak, and J. Chen, "An analysis of conductor surface roughness effects on signal propagation for stripline interconnects," *IEEE Trans. Electromagn. Compat.*, vol. 56, no. 3, pp. 707–714, Jun. 2014.
- [4] S. Yong et al., "A cross-sectional profile based model for stripline conductor surface roughness," in *Proc. IEEE Int. Symp. Electromagn. Compat. Signal/Power Integrity*, 2020, pp. 334–339.
- [5] E. Hammerstad and O. Jensen, "Accurate models for microstrip computeraided design," in *Proc. IEEE MTT-S Int. Microw. Symp. Dig.*, 1980, pp. 407–409.
- [6] S. Hall et al., "Multigigahertz causal transmission line modeling methodology using a 3-D hemispherical surface roughness approach," *IEEE Trans. Microw. Theory Techn.*, vol. 55, no. 12, pp. 2614–2624, Dec. 2007.
- [7] E. Bogatin, D. DeGroot, P. G. Huray, and Y. Shlepnev, "Which one is better? Comparing options to describe frequency dependent losses," DesignCon. 2013.
- [8] J. J. Ellison and S. Agili, "In situ stripline laminate property extraction accounting for effective surface roughness losses," in *Proc. IEEE Int. Symp. Electromagn. Compat. Signal/Power Integrity*, 2017, pp. 198–202.
- [9] S. Jin, B. Chen, X. Fang, H. Gao, X. Ye, and J. Fan, "Improved "root-omega" method for transmission-line-based material property extraction for multilayer PCBs," *IEEE Trans. Electromagn. Compat.*, vol. 59, no. 4, pp. 1356–1367, Aug., 2017.
- [10] M. T. Serrano-Serrano and R. Torres-Torres, "Causal model implementation for the conductor surface roughness effect on the attenuation and delay of microstrip lines," *IEEE Trans. Microw. Theory Techn.*, vol. 72, no. 1, pp. 64–73, Jan., 2024.
- [11] Z. Sun, J. Liu, X. Xiong, V. Khilkevich, D. Kim, and D. Beetner, "Extraction of stripline surface roughness using cross-section information and s-parameter measurements," in *Proc. IEEE Int. Symp. Electromagn. Compat. Signal/Power Integrity*, pp. 80–85, 2022.
- [12] D. M. Pozar, *Microwave Engineering*. Hoboken, NJ, USA: Wiley, 2011.
- [13] P. G. Huray, The Foundations of Signal Integrity. Hoboken, NJ, USA: Wiley, 2009.
- [14] B. Chen, X. Ye, B. Samaras, and J. Fan, "A novel de-embedding method suitable for transmission-line measurement," in *Proc. Asia-Pacific Symp. Electromagn. Compat.*, 2015, pp. 1–4.
- [15] S. Yong et al., "Dielectric loss tangent extraction using modal measurements and 2-D cross-sectional analysis for multilayer PCBs," IEEE Trans. Electromagn. Compat., vol. 62, no. 4, pp. 1278–1292, Aug. 2020.
- [16] J. Li, Y. Liu, L. Liu, S. Xia, S. Hinaga, and V. Khilkevich, "Dielectric loss tangent extraction using two single-ended striplines of different width," in *Proc. IEEE Int. Symp. Electromagn. Compat. Signal/Power Integrity*, 2022, pp. 86–91.
- [17] C. Audet, Dennis Jr, and J. E., "Analysis of generalized pattern searches," SIAM J. Optim., vol. 13, no. 3, pp. 889–903, 2002.
- [18] S. De, A. Gafarov, M. Y. Koledintseva, R. J. Stanley, J. L. Drewniak, and S. Hinaga, "Semi-automatic copper foil surface roughness detection from PCB microsection images," in *Proc. IEEE Int. Symp. Electromagn. Compat.*, 2012, pp. 132–137.